Available online at BCREC Website: https://bcrec.undip.ac.id

Bulletin of Chemical Reaction Engineering & Catalysis, 13 (1), 2018, 170-178

Research Article

CeO_2-TiO_2 Photocatalyst: Ionic Liquid-Mediated Synthesis, Characterization, and Performance for Diisopropanolamine Visible Light Degradation

Jagath Retchahan Sivalingam, Chong Fai Kait*, Cecilia Devi Wilfred

Fundamental and Applied Sciences Department, Universiti Teknologi PETRONAS, 32610 Seri Iskandar, Perak Darul Ridzuan, Malaysia

Received: 26th July 2017; Revised: 22nd October 2017; Accepted: 29th October 2017; Available online: 22nd January 2018; Published regularly: 2nd April 2018

Abstract

CeO_2-TiO_2 photocatalyst with Ce:Ti molar ratio of 1:9 was synthesized via co-precipitation method in the presence of 1-ethyl-3-methyl imidazolium octylsulfate, [EMIM][$OctSO_4$] (CeO_2-TiO_2-IL). The ionic liquid acts as a templating agent for particle growth. The CeO_2-TiO_2 and TiO_2 photocatalysts were also synthesized without any ionic liquid for comparison. Calcination was conducted on the as-synthesized materials at 400 ˚C for 2 h. The photocatalysts were characterized using diffuse reflectance UV-Vis spectroscopy (DR-UV-Vis), field emission scanning electron microscopy (FESEM), X-ray powder diffraction (XRD), and surface area and pore size analyzer (SAP). The presence of CeO_2 has changed the optical property of TiO_2. It has extended the absorption edge of TiO_2 from UV to visible region. The calculated band gap energy decreased from 2.82 eV (TiO_2) to 2.30 eV (CeO_2-TiO_2-IL). The FESEM morphology showed that samples forms aggregates and the surface smoothens when ionic liquid was added. The average crystallite size of TiO_2, CeO_2-TiO_2, and CeO_2-TiO_2-IL were 20.8 nm, 5.5 nm, and 4 nm. In terms of performance, photodegradation of 1000 ppm of diisopropanolamine (DIPA) was conducted in the presence of hydrogen peroxide (H_2O_2) and visible light irradiation which was provided by a 500 W halogen lamp. The best performance was displayed by CeO_2-TiO_2-IL calcined at 400 ˚C. It was able to remove 82.0% DIPA and 54.8% COD after 6 h reaction.

Keywords: TiO_2; CeO_2; DIPA; ionic liquid; photocatalyst

How to Cite: Sivalingam, J.R., Kait, C.F., Wilfred, C.D. (2018). CeO_2-TiO_2 Photocatalyst: Ionic Liquid-Mediated Synthesis, Characterization, and Performance for Diisopropanolamine Visible Light Degradation. *Bulletin of Chemical Reaction Engineering & Catalysis*, 13 (1): 170-178 (doi:10.9767/bcrec.13.1.1396.170-178)

Permalink/DOI: https://doi.org/10.9767/bcrec.13.1.1396.170-178

1. Introduction

Diisopropanolamine (DIPA) is widely employed in processing facilities; acidic and impurity gases namely carbon dioxide, hydrogen sulfide are removed using amine gas treating or gas sweetening process. Raw natural gas consists of hydrocarbons, acidic and impurity gases [1]. Photocatalysis has attracted much attention in solving environmental issues. In order to process the gases, alkanolamine substances are used, namely monoethanolamine, diethanolamine, methyldiethanolamine, and diisopropanolamine [2]. Completion and recycling stage of process involves removal or recycling of alka-

* Corresponding Author.
E-mail: chongfaikait@utp.edu.my (Kait, C.F.)

nolamine. Some of the alkanolamines are not converted or deposited in the system and might even be carried into the wastewater system endangering the biological systems in water [1].

Current research focuses on TiO_2 which is used to photodegrade DIPA via advanced oxidation process (AOP) [3]. Bimetallic catalyst was used as well to study the alkanolamine degradation. This includes Cu-Fe-TiO_2 and Cu-Ni/TiO_2 photocatalyst study on DIPA degradation under visible light [2,4]. TiO_2 has been widely employed as an important ingredient in industrial products such as paints, polymer products, and textile industry. TiO_2 is non-flammable, heat stable, and classified as non-hazardous [5]. Photo-catalytic activity involves excitation of a material by a photon from light source followed by chemical reaction. The principle involves the generation of electron hole pairs for oxidation or reduction reactions [6]. Anatase TiO_2 has a wide band gap of 3.2 eV with an absorption edge at 388 nm. It can absorb UV region of about 4% solar radiation. In contrast solar spectrum gives 40% visible region and the wavelength range is 400-700 nm [7].

In order to enhance photocatalyst performance, modification to semiconductors is done to improve radiation absorption into the visible region. Some CeO_2 metal oxide doping is one approach [8]. TiO_2 mixed with CeO_2 was able to perform better compared to other photocatalysts. The CeO_2 is a semiconductor with varying band gap energy from 2.7 eV to 3.4 eV based on the preparation methods [9]. The coupling of these oxides aids in the migration of photo-excited electrons from the valence band of TiO_2 to CeO_2 upon irradiation. This decreases the charge recombination between the two metal oxides and enhances the photocatalytic activity [10]. In addition, the presence of CeO_2 decreases the overall band gap energy (eV) and acts as electron traps as it reduces electron hole recombination rate of photocatalysts [9].

Besides doping, photocatalyst synthesized via ionic liquid-assisted method displayed promising performance compared to without ionic liquid. The use of halide-free (sulfate anion) is environmentally friendly [11]. Octyl sulfate ionic liquids are primary choice ionic liquids for their promising industrial reactions and cheap cost of synthesis [12]. Ionic liquid-mediated synthesis of CeO_2-TiO_2 has been conducted using [C_{16}mim] Br for *p*-chlorophenol dye degradation. It was proven to display better photo-activity under both UV/visible-light irradiation, with degradation rate of 95.3% [13]. The presence of ionic liquid produced a low surface tension system which results in increased nucleation level and thus aids in small particle growth. It also creates better surface tension aids in catalysis process where it deals mainly on adsorption and desorption of a material onto a catalyst [11]. It also affects particle morphology [14]. The presence of sulfate anion in ionic liquid enhances the structural property and performance of the photocatalyst [11].

Ceria has attracted much attention due to its strong oxidizing power [15], which is an important requirement for photodegradation of DIPA. When Ce^{3+} is doped onto TiO_2, the photoresponse of the materials could be extended into the visible region, which allows the possibility of utilizing the free and abundant sunlight for the photodegradation process. Therefore, the novelty of the work involved ionic liquid-mediated synthesis of CeO_2-TiO_2 using 1-ethyl-3-methylimidazolium octylsulfate, [EMIM][OctylSO_4], and its application for photodegradation of diisopropanolamine (DIPA) under visible light radiation. To date, no work has been reported on the same system for the photodegradation of DIPA. The objective includes investigating the effect of the presence of ionic liquid, 1-ethyl-3-methyl imidazolium octylsulfate, [EMIM][OctSO_4] during synthesis of CeO_2-TiO_2 on the photocatalyst properties and photodegradation of DIPA.

2. Materials and Methods

2.1 Materials

All chemicals were used as received. Titanium tetrachloride ($TiCl_4$, 99.90%), ammonia solution [NH_3 (aq), 25%], diisopropanolamine [C_3H_9NO] (98%), hydrogen peroxide [H_2O_2] (30%), 1-ethyl-3-methylimidazolium octylsulfate [$C_{14}H_{28}N_2O_4S$] (99%), sodium hydroxide [NaOH] (99%), and sodium dihydrogen phosphate [NaH_2PO_4] (99%), were purchased from Merck. Cerium(III) nitrate hexahydrate [$Ce(NO_3)_3.6H_2O$] (99%) was purchased from Sigma-Aldrich.

2.2 Methods

2.2.1 Synthesis of CeO_2-TiO_2

CeO_2-TiO_2 photocatalyst with Ce:Ti molar ratio of 1:9 was synthesized in the presence of [EMIM][OctSO_4]. Approximately 0.1 mol of Ce^{3+} was mixed with 3 mL of [EMIM][OctSO_4] ionic liquid in 40 mL of deionized water (DI). $TiCl_4$ was added dropwise to the mixture with continuous stirring in a beaker immersed in an ice bath. Ammonia solution was added to pre-

cipitate the mixed oxides forming a light yellowish solid in 5 minutes duration. Synthesis was conducted at room temperature and pressure (RTP), continuous stirring for 2 h throughout synthesis. The precipitate was filtered, washed few times using distilled water. During washing, samples were mixed with adequate amount of water and stirred for 5 minutes. This step was repeated multiple times until chloride (determined using chloride probe) is absent in photocatalyst. Samples was then dried overnight at 70˚C. The as-synthesized material was ground and calcined at 400˚C for 2 h. TiO_2, CeO_2-TiO_2 (samples without ionic liquid addition) were synthesized as per similar condition and procedure as mentioned above excluding addition of ionic liquid section. TiO_2, CeO_2-TiO_2 denotes photocatalysts without [EMIM][$OctSO_4$] presence, whereas CeO_2-TiO_2-IL denotes photocatalysts with [EMIM][$OctSO_4$] for comparison purpose.

2.2.2 Sample characterization

The diffuse reflectance-UV visible (DR-UV-Vis) spectra of all photocatalysts were recorded using Cary 100 (Agilent) spectrophotometer and spectralon was used as a reference. Field Emission Scanning Electron Microscope (FESEM) was conducted using Zeiss Supra55 VP to determine sample morphology which was operated at 100 kx magnification. X-ray powder diffraction (XRD), was conducted using X'Pert Powder, PANalytical, and surface area/pore size were determined using Micromeritics ASAP 2020, Agilent 1100 High Performance Liquid Chromatography (HPLC) was used to determine DIPA concentration and COD digester (HACH DRB200) was used for COD vial digestion.

2.2.3 DIPA photodegradation

The initial concentration of DIPA was 1000 ppm and the photocatalyst dosage was 0.1 g/L. Dark reaction was carried out for one hour to ensure equilibration between DIPA and the photocatalyst prior to photo-degradation under the irradiation of halogen lamp (500W) for 6 h in the presence of H_2O_2. The 0.01 g of photocatalyst was added into 100 mL DIPA followed by 4 mL of H_2O_2 for the first 1 h. After 1 h, another 4 mL H_2O_2 was added into the reaction mixture and the addition was repeated every hour for 6 h in total. The H_2O_2 addition follows 1mol DIPA to 16 mol H_2O_2 as referred to Eq.1. At the end of the reaction, the DIPA level was determined using Agilent 1100 High Performance Liquid Chromatography (HPLC) using sodium dihydrogen phosphate (NaH_2PO_4) and sodium hydroxide (NaOH) as the mobile phase. Chemical oxygen demand (COD) was determined using COD digester (digestion) followed by DR 5000. The percentage removal was then determined using Equations 2 and 3, respectively.

$$C_6H_{15}NO_2+16H_2O_2 \rightarrow 6CO_2+22H_2O+ NH_3 \quad (1)$$

$$COD\ removal\ (\%)= (COD_i\text{-}COD_f)/COD_i \times 100 \quad (2)$$

$$DIPA\ removal\ (\%) = (DIPA_i\text{-}DIPA_f)/DIPA_i \times 100 \quad (3)$$

Where COD_i and COD_f are the initial and final COD concentrations, respectively of aqueous DIPA solution (ppm). Meanwhile, $DIPA_i$ and $DIPA_f$ are the initial and final DIPA concentrations, respectively of aqueous DIPA solution (ppm).

3. Results and Discussion

3.1 Characterization

Figure 1 shows X-ray powder diffraction pattern of TiO_2, CeO_2-TiO_2, and CeO_2-TiO_2-IL calcined at 400 °C for 2 h. The diffraction peak values for TiO_2 are 25.2°, 37.8°, 54.4°, 54.3°, 56.7°, 64.2°, 69.0°, 70.3°, and 76.0° with its corresponding (101), (004), (200), (105), (116), (211), and (215) planes, respectively. Minor Ce peaks have been observed at 28.5°, 33.0°, and 69.7° for Figure 1 (c) followed by peak at 69.6° for Figure 1 (b). Peaks at 69.6° Figure 1 (b), and 69.7° for Figure 1 (c) corresponds to mixture of Ce and Ti peaks overlapping with peaks at 69.0° Figure 1 (a). From the Figure 1 it shows that only anatase phase of TiO_2 was ob-

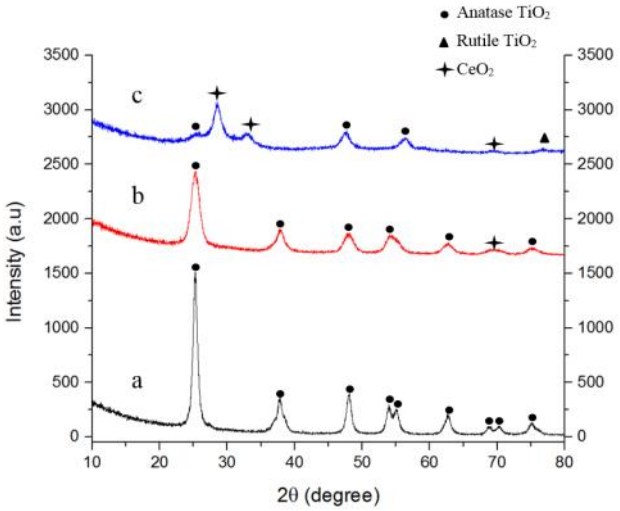

Figure 1. The XRD patterns of (a) TiO_2 (b) CeO_2-TiO_2 (c) CeO_2-TiO_2-IL calcined at 400°C for 2 h

served. It implies that addition of Ce and ionic liquid allows dispersion of Ce on TiO_2 without altering the phase of TiO_2 where anatase phase was stabilized to a level [16]. Smaller amount of Ce crystalline phase was observed due to little amount of Ce present in the sample and with the hike up to 10% of CeO_2 in the sample, diffraction peaks of CeO_2 is slowly visible [17].

Addition of Ce and ionic liquid further reduces the peak intensity to a minimum. It broadens and widens the peak. It indicates formation of finer crystals than pure compound [13]. Besides that, it is also due to the growth of TiO_2 being inhibited as adding Ce. This creates ample amount of defects namely oxygen vacancies in the crystal thus inhibits the crystal growth [17]. This scenario can be used for ionic liquid addition as well. The crystalline size was calculated using Debye-Scherrer equation (Equation (4)).

$$D = 0.9\lambda/(\beta \cos \theta) \quad (4)$$

where λ is the wavelength, D is the crystallite size, θ is the diffraction angle, and β is the FWHM.

Crystallinity was observed to decrease for CeO_2-TiO_2 as estimated by the broad, low intensity peak at 25.2° for the (101) anatase plane [18]. The average crystallite size of TiO_2, CeO_2-TiO_2, and CeO_2-TiO_2-IL are 20.8 nm, 5.5 nm, and 4 nm. It corresponds with the peak intensity obtained as well. The peak at (101) is observed to be un-shifted for Figure 1 (a,b) and shifted to the right for Figure 1 (c). The unshifting might be due to presence of minimal amount of Ce as ratio or it does not incorporated into TiO_2 [18]. In addition, Ce could be present or located on the TiO_2 surface, as a cluster or agglomerate [18]. The shifting is due to deformations in lattice structure of TiO_2 that is formed as adding Ce to it [17]. It alters the lattice structure of TiO_2 and forms new energy level.

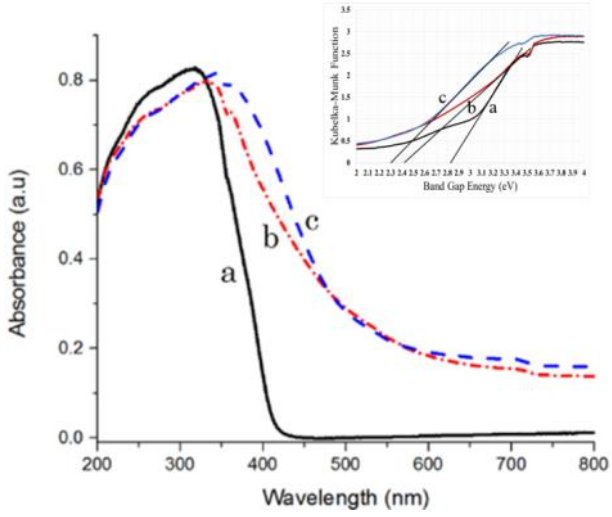

Figure 2. Diffuse reflectance visible spectra plotted as the Kubelka-Munk function of (a) TiO_2, (b) CeO_2-TiO_2, and (c) CeO_2-TiO_2-IL

Figure 2 shows the DR-UV-Vis spectra for TiO_2, CeO_2-TiO_2, and CeO_2-TiO_2-IL. The TiO_2 records no significant absorbance from 400 nm onwards with band gap energy of 2.82 eV. The spectrum shows spectral response towards visible region which is from 400-650 nm for CeO_2-TiO_2 and CeO_2-TiO_2-IL. The graph observed to be skewed towards right (red shift) to a longer wavelength in for graphs Figure 2 (b) and (c). Looking into the band gap energy, it decreases with the presence of cerium and ionic liquid [EMIM][$OctSO_4$].

Referring to Table 1, the presence of CeO_2 decreased the band gap energy of TiO_2 from 2.82 eV to 2.30 eV. The slight deviation in the band gap TiO_2 value from actual reported value (3.2 eV - anatase) is due to oxygen vacancies that might be responsible for defective states on TiO_2 interface and as well preparation method [19]. The lower band gap of CeO_2-TiO_2 may indicate strong interaction between CeO_2 and TiO_2 that induced synergistic effect that could not be displayed if the materials are physically mixed [20]. Lower overall band gap can be explained in terms CeO_2 substitution creates new energy level at partially filled Ce 4f level in between valence and conduction band of TiO_2 [21]. It reduces electron-hole pair recombination rate and improves the efficiency of interfacial charge-transfer from impurity to conduction level [22]. This decreases the overall band gap energy. The presence of CeO_2-TiO_2 and TiO_2 anatase and rutile composition in the catalyst increases the charge separation between the molecules and thus giving sharper/narrow absorption curve [19]. During sample preparation, ratio of 1:9 has been used for CeO_2:TiO_2.

Figure 3 shows the (FESEM) of TiO_2, CeO_2-TiO_2, and CeO_2-TiO_2-IL calcined at 400˚C at 100 kX magnification. Rod shaped particles

Table 1. Band gap values of the photocatalysts

Photocatalyst	Band Gap (eV)
TiO_2	2.82
CeO_2-TiO_2	2.43
CeO_2-TiO_2-IL	2.30

which are stacked side by side are been observed in Figure 3 (a) for TiO_2 gives nanoparticles average size ranged from 16.6-59.3 nm. Rod shaped particle which are stacked side by side has been observed. It follows the size range of 20-30 nm for TiO_2 [19]. The CeO_2-TiO_2 showed agglomeration of particles with diameter ranging from 9.9-10.5 nm. The FESEM images for CeO_2-TiO_2-IL recorded nanoparticles

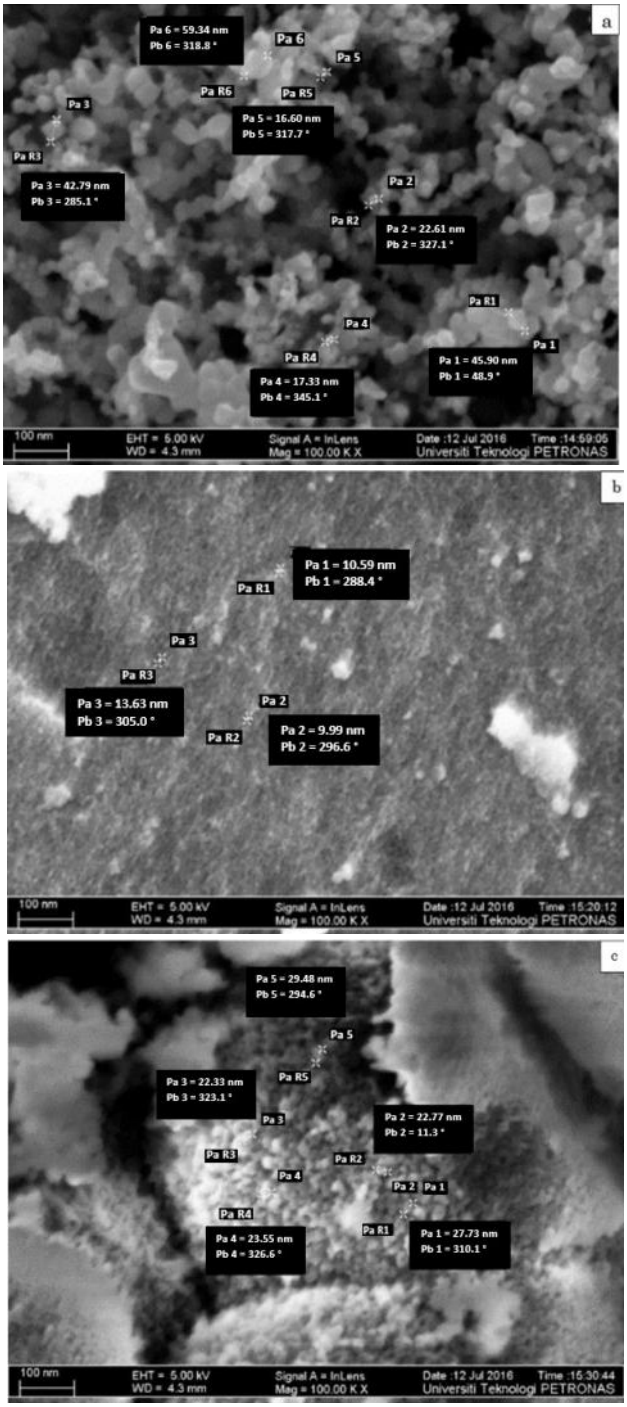

Figure 3. FESEM images for (a) TiO_2 (b) CeO_2-TiO_2 and (c) CeO_2-TiO_2-IL at 100 kX magnification

average size range of about 22.7-29.4 nm. It recorded to have lumped form particles sticked together in a spherical shape. Aggregate of white substance has been spotted on the electron image of the particles, covering the lump particles as referred to Figure 3 (b) and (c). In this research, it follows precipitation method. Observed from FESEM images that CeO_2-TiO_2 were spherical in shape and is about 10-15 nm in size [8]. Aggregates of particles, forms chain-like structure and lumps, with the sizes ranging from 40 nm to 1 µm [18]. Similarly, in this research CeO_2-TiO_2 sample forms chain like structure with no aggregates. The sizes are in the range from 9 nm to 11 nm. Upon adding ionic liquid, the aggregation intensifies, forming bigger spherical shaped particles. The particle size increased as the result of the presence of IL.

Table 2 shows the porosity and surface area of mesoporous TiO_2, CeO_2-TiO_2, and CeO_2-TiO_2-IL nanoparticles characterized using nitrogen adsorption and desorption isotherms. CeO_2-TiO_2-IL recorded highest BET surface area value of 148.2 m^2/g. Pore diameter and volume seems to be decreased as adding Ce^{3+} and ionic liquid to TiO_2. BET surface area value observed to be increasing in trend as adding Ce^{3+} and ionic liquid to TiO_2. Figure 4 (a) shows type III isotherm pattern whereas the rest of the samples has type IV isotherm curves. The pattern difference is due to intercalation and expansion of structure layers and the entry of activated molecules via smaller pore entrance pathways [23].

Hysteresis loop has been observed in adsorption and desorption branch at varies level of pressure (*P*/*Po*). It shows that each curve has two definite region where at low relative pressure, the isotherms gives higher adsorption which confirms the presence of micropores (type I). In contrast, at higher relative pressure, the curves shows hysteresis loop, this confirms the presence of mesopores (type IV) at 0.4 *P*/*Po*. Sharp "knee" point at *P*/*Po* 0.01-0.03, 0-0.02, and 0-0.03 was observed for Figure 4 (a), (b), and (c). This point gives monolayer ca-

Table 2. Pore size distribution

Samples	Surface Area, m^2/g	Pore Diameter, Å	Pore Volume, cm^3/g
TiO_2	48.5	159.3	0.19
CeO_2-TiO_2	121.1	38.7	0.11
CeO_2-TiO_2-IL	148.2	37.3	0.16

pacity measure where the surface area adsorbent been determined [24]. Monolayer-multilayer adsorption is observed at low *P*/*Po*. Sharp rise in isotherm slope been observed at *P*/*Po* above 0.9-1.0, 0.97-1.0, and 0.95-1.0 for Figure 4 (a), (b), and (c). This is due to condensation and saturation of capillaries present within the pores [25].

Pores can be divided into three groups namely micropore (2 nm), mesopore (2-50 nm) and macropore (>50 nm) with their respective diameter categories [24]. The pore size distributions for TiO_2, CeO_2-TiO_2 and CeO_2-TiO_2-IL are 5-49 nm, 5-80 nm, and 5-85 nm. Since the pore size value is at upper mesopore and lower macropore margin, condensation and isotherm rise happens at high *P*/*Po* region [24]. It summarizes that the samples has mesopore category. Pore volume and pore diameter shows that TiO_2 has the highest value, 159.3 Å and 0.19 cm^3/g, compared to other samples. This is because TiO_2 might have blocked the active sites pores resulting in low pore volume and diameter in other samples [26]. Besides that nitrate and cerium ions might adsorbed on TiO_2 and inhibit the TiO_2 growth. This resulted in small pore diameter and volume in the sample [27]. This can be related to Table 2. Pore size and pore volume considered to be less important parameter in deciding the photocatalytic activity [26].

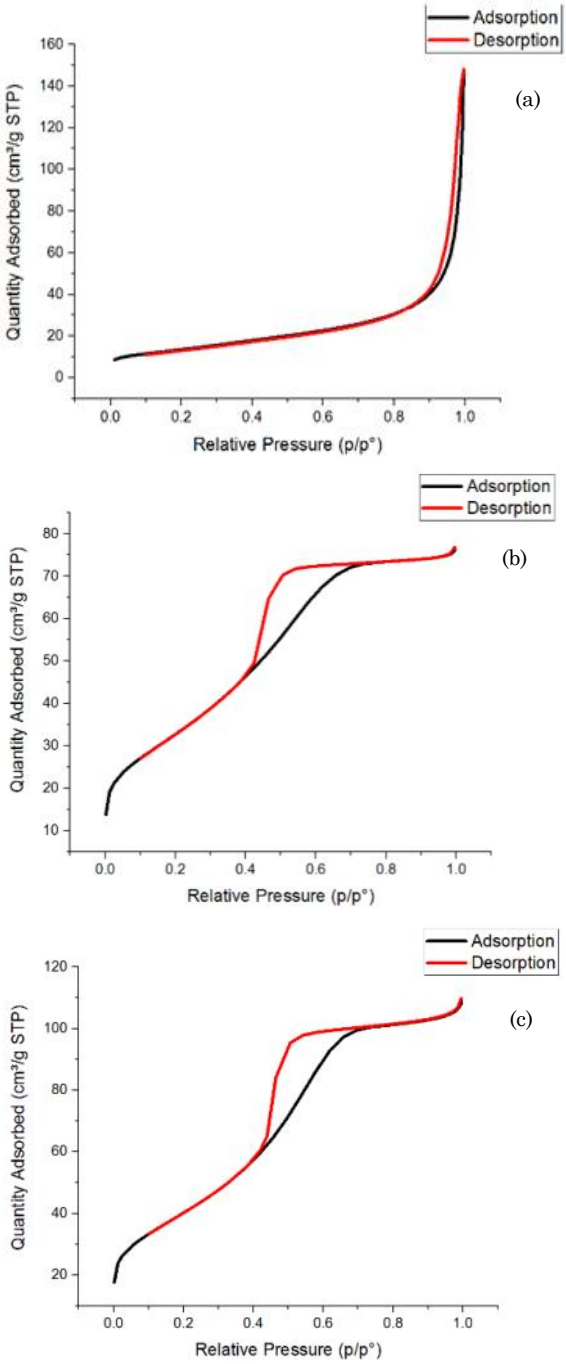

Figure 4. Nitrogen adsorption isotherm pattern of (a) TiO_2, (b) CeO_2-TiO_2, (c) CeO_2-TiO_2-IL calcined at 400 °C for 2 h

The surface area seems to be higher for CeO_2-TiO_2-IL (3 mL), 148.2 m^2/g. Smaller pore size was observed for CeO_2-TiO_2 (38.7 Å) and CeO_2-TiO_2-IL (3 mL) (37.3 Å). High surface area is due to the ionic liquid and Ce presence which limits the CeO_2-TiO_2 agglomeration. Higher surface area of sample also implies the presence of finer particles of the sample [28]. Smaller pore size implies formation of finer and smoother particles. Similar situation can be observed when adding cerium, surface area increases whereas pore volume and diameter decreases gradually [27]. This can followed as well for ionic liquid addition. Besides that, all the samples shows hysteresis loop which has bimodal pore size distribution. This is due to two different type of aggregation in the samples; one is the finer intra-aggregated pore whereas the other one is the bigger inter-aggregated pore [28]. This could be due to particle size and shape which has influenced the structure of the pore [28]. The hysteresis loop is due to capillary condensation of mesoporous sample [29]. The pore volume and diameter plays crucial role in determining the performance of the catalyst [30]. It determines the loading and adsorption of pollutant to be degraded. TiO_2 pore volume and diameter stated to be 0.29 cm^3/g and 21.9 nm [30]. Similarly from this test, it gives 0.19 and (15.9 nm or 159 Å) for TiO_2 pore volume and diameter. The variation might be from preparation method. The main factor that plays key role are pore surface area and crystallinity of the photocatalyst.

3.2 Photocatalytic degradation reaction

Figure 5 shows the photo-catalytic performance of TiO_2, CeO_2-TiO_2, and CeO_2-TiO_2-IL in DIPA degradation which was conducted under halogen lamp (500W). Referring to DIPA, it has reduced up to 66.0%, 75.0%, and 82.0% (final light reaction). As CeO_2 is doped to TiO_2 the photo-catalytic DIPA and COD degradation shows escalation in degradation and when ionic liquid is added, the performance increases further. COD removal of about 43.2%, 42.7%, and 54.8% has been recorded for TiO_2, CeO_2-TiO_2, and CeO_2-TiO_2-IL, respectively. Smaller particle size, high surface area, as well as lower band gap energy enhances the excitation of electrons from one level to another as well. This gives better photo-degradation of DIPA and COD removal. It agrees with the acute toxicity <289 mg/L [31].

4. Conclusions

FESEM images characterization shows that the nanoparticles are in nanorange. The average crystallite sizes decreased from 20.8 nm to 5.5 nm, and 4 nm as adding Ce and ionic liquid to TiO_2. Lower band gap energy of CeO_2-TiO_2 (2.43 eV) and CeO_2-TiO_2-IL (2.30 eV) has been observed as well. The particle size of TiO_2 decreased from 59.3 nm to 9.9 nm, and 22.7 nm as adding Ce and ionic liquid. The sample as well are mostly mesopore in sizes. The photo-degradation performance studies showed that CeO_2-TiO_2-IL has better DIPA degradation and COD removal level of about 82.0% and 54.8% respectively. The present synthesized photo-catalyst with the addition ethyl imidazolium octyl sulfate ionic liquid is proven to be more effective for aqueous DIPA degradation and COD removal. This is due to better surface property of the synthesized catalyst. This indicates the synthesized sample can be an ideal choice of catalyst for application in photo-degradation studies and provides the knowledge of utilizing solar spectrum with wide range of wavelength effectively. Thus it gives new scope in designing, optimizing and utilizing photocatalyst system.

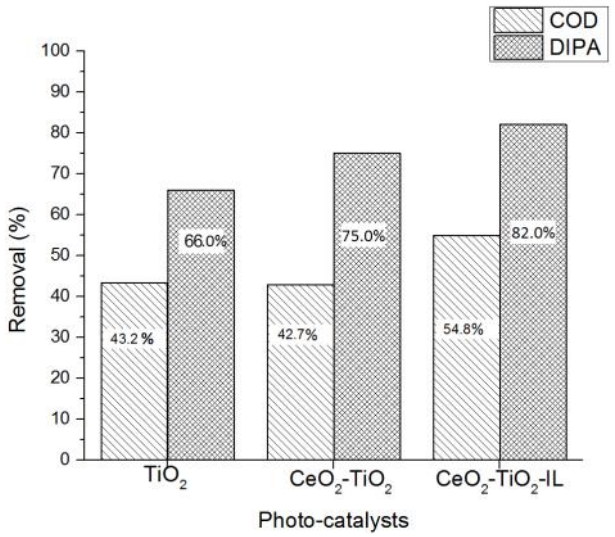

Figure 5. DIPA and COD removal percentage for photocatalysts at room temperature and pressure (RTP)

Acknowledgement

The authors acknowledge the support provide by the Centre of Research in Ionic Liquids (CORIL), Universiti Teknologi PETRONAS, Malaysia.

References

[1] Hansen, B.H., Altin, D., Booth, A., Vang, S. H., Frenzel, M., Sørheim, K.R., Størseth, T.R. (2010). Molecular effects of diethanolamine exposure on Calanus finmarchicus (Crustacea: Copepoda). *Aquatic Toxicology*, 99(2): 212-222.

[2] Ramli, R.M., Kait, C.F., Omar, A.A. (2016). Remediation of DIPA Contaminated Wastewater Using Visible Light Active Bimetallic Cu-Fe/TiO_2 Photocatalyst. *Procedia Engineering*, 148: 508-515.

[3] Ramli, R.M., Chong, F.K., Omar, A.A., Murugesan, T. (2015). Performance of surfactant assisted synthesis of Fe/TiO_2 on the photodegradation of diisopropanolamine. *CLEAN–Soil, Air, Water*, 43(5): 690-697.

[4] Riaz, N., Bustam, M.A., Chong, F.K., Man, Z.B., Khan, M.S., Shariff, A.M. (2014). Photocatalytic Degradation of DIPA Using Bimetallic Cu-Ni/TiO_2 Photocatalyst under Visible Light Irradiation. *The Scientific World Journal*. 2014: 342020-342020

[5] (TDMA) Titanium Dioxide Manufacturers Association. (2012). About Titanium Dioxide. *Citing Internet sources* URL http://www.cefic.org/Documents/Industry%20sectors/TDMA/about-TiO_2-fullversion-July-2013.pdf.

[6] Khang, N.C., Van, M.N., Yang, I.S. (2011). Synthesis and characterization of the N-doped TiO_2 photocatalyst for the photodegradation of methylene blue and phenol. *Journal of Nanoscience and Nanotechnology*, 11(7): 6494-6498.

[7] Rhodia. (2012). Cerium Dioxide. *Citing Internet sources* URL http:www.solvay.com/en/ binaries/Cerium_Dioxide_GPS_rev0_Sept12_RHD-139543.pdf.

[8] Magesh, G., Viswanathan, B., Viswanath, R. P., Varadarajan, T.K. (2009). Photocatalytic behavior of CeO_2-TiO_2 system for the degradation of methylene blue. *Indian journal of Chemistry. Section A: Inorganic, Physical, Theoretical & Analytical*. 48(4): 480-488

[9] Fiorenza, R., Bellardita, M., D'Urso, L., Compagnini, G., Palmisano, L., Scirè, S. (2016). Au/TiO_2-CeO_2 Catalysts for Photocatalytic Water Splitting and VOCs Oxidation Reactions. *Catalysts*, 6: 121

[10] Plechkova, N.V., Seddon, K.R. (2008). Applications of ionic liquids in the chemical industry. *Chemical Society Reviews*, 37(1): 123-150.

[11] González, B., Gómez, E., Domínguez, A., Vilas, M., Tojo, E. (2010). Physicochemical characterization of new sulfate ionic liquids. *Journal of Chemical & Engineering Data*, 56(1): 14-20.

[12] Sherly, E.D., Vijaya, J.J., Kennedy, L.J. (2015). Effect of CeO_2 coupling on the structural, optical and photocatalytic properties of ZnO nanoparticle. *Journal of Molecular Structure*, 1099: 114-125.

[13] Liu, H., Wang, M., Wang, Y., Liang, Y., Cao, W., Su, Y. (2011). Ionic liquid-templated synthesis of mesoporous CeO_2-TiO_2 nanoparticles and their enhanced photocatalytic activities under UV or visible light. *Journal of Photochemistry and Photobiology A: Chemistry*, 223(2): 157-164.

[14] Nan, A., Liebscher, J. (2011). Ionic liquids as advantageous solvents for preparation of nanostructures. In: Handy S (ed) *Applications of ionic liquids in science and technology*. Pub InTech, Rijeka, Croatia, Chapter 14, pp. 287–301

[15] Miao, S., Liu, Z., Miao, Z., Han, B., Ding, K., An, G., Xie, Y. (2009). Ionic liquid-mediated synthesis of crystalline CeO_2 mesoporous films and their application in aerobic oxidation of benzyl alcohol. *Microporous and Mesoporous Materials*, 117: 386-390.

[16] Abdullah, H., Khan, M.R., Pudukudy, M., Yaakob, Z., Ismail, N.A. (2015). CeO_2-TiO_2 as a visible light active catalyst for the photoreduction of CO_2 to methanol. *Journal of Rare Earths*, 33(11): 1155-1161.

[17] Li, W., Wang, Y., Ji, B., Jiao, X., Chen, D. (2015). Flexible Pd/CeO_2-TiO_2 nanofibrous membrane with high efficiency ultrafine particulate filtration and improved CO catalytic oxidation performance. *RSC Advances*, 5(72): 58120-58127.

[18] Zuas, O., Hamim, N. (2013). Synthesis, Characterization and Properties of CeO_2-doped TiO_2 Composite Nanocrystals. *Materials Science*, 19(4): 443-447.

[19] Verma, R., Samdarshi, S.K., Singh, J. (2015). Hexagonal Ceria Located at the Interface of Anatase/Rutile TiO_2 Superstructure Optimized for High Activity under Combined UV and Visible-Light Irradiation. *The Journal of Physical Chemistry C*, 119(42): 23899-23909.

[20] Vijayalakshmi, R., Rajendran, V. (2012). Synthesis and characterization of nano-TiO_2 via different methods. *Archives of Applied Science Research*, 4(2), 1183-1190.

[21] Singh, M.P., Mandal, S.K., Verma, Y.L., Gupta, A.K., Singh, R.K., Chandra, S. (2014). Viscoelastic, surface, and volumetric properties of ionic liquids [BMIM][$OcSO_4$] [BMIM][PF_6], and [EMIM][$MeSO_3$]. *Journal of Chemical & Engineering Data*, 59(8): 2349-2359.

[22] Xu, A.W., Gao, Y., Liu, H.Q. (2002). The preparation, characterization, and their photocatalytic activities of rare-earth-doped TiO_2 nanoparticles. *Journal of Catalysis,* 207: 151-157.

[23] Sing, K., Williams, R. (2004). Physisorption hysteresis loops and the characterization of nanoporous materials. *Adsorption Science & Technology*, 22(10): 773-782.

[24] Tan, Y.H., Davis, J.A., Fujikawa, K., Ganesh, N.V., Demchenko, A.V., Stine, K.J. (2012). Surface area and pore size characteristics of nanoporous gold subjected to thermal, mechanical, or surface modification studied using gas adsorption isotherms, cyclic voltammetry, thermogravimetric analysis, and scanning electron microscopy. *Journal of Materials Chemistry*, *22*(14): 6733-6745.

[25] Kumar, D.A., Shyla, J.M., Xavier, F.P. (2012). Synthesis and characterization of TiO_2/SiO_2 nano composites for solar cell applications. *Applied Nanoscience*, 2(4): 429-436.

[26] Sayari, A., Jaroniec, M. (2002). Nanoporous materials III. Elsevier.

[27] Wang, Y., Zhao, J., Wang, T., Li, Y., Li, X., Yin, J., Wang, C. (2016). CO_2 photoreduction with H_2O vapor on highly dispersed CeO_2/TiO_2 catalysts: Surface species and their reactivity. *Journal of Catalysis*, 337: 293-302.

[28] Fang, J., Bao, H., He, B., Wang, F., Si, D., Jiang, Z., Huang, W. (2007). Interfacial and surface structures of CeO_2-TiO_2 mixed oxides. *The Journal of Physical Chemistry C*, 111(51): 19078-19085.

[29] Lopez, T., Rojas, F., Alexander-Katz, R., Galindo, F., Balankin, A., Buljan, A. (2004). Porosity, structural and fractal study of sol–gel TiO_2-CeO_2 mixed oxides. *Journal of Solid State Chemistry*, 177(6): 1873-1885.

[30] Gaol, F.L., Webb, J. (Eds.). (2014). *Recent Trends in Nanotechnology and Materials Science: Selected Review Papers from the 2013 International Conference on Manufacturing, Optimization, Industrial and Material Engineering (MOIME 2013)*. Springer.

[31] CCME. (2007). Canadian soil quality guidelines for the protection of environmental and human health: summary tables.